Effect of Strain Rate on Stress-Strain Behavior of Alloy 309 and 304L Austenitic Stainless Steel

JOSHUA A. LICHTENFELD, MARTIN C. MATAYA, and CHESTER J. VAN TYNE

The effect of strain rate on stress-strain behavior of austenitic stainless steel 309 and 304L was investigated. Tensile tests were conducted at room temperature at strain rates ranging from $1.25 \times 10^{-4}\ s^{-1}$ to $400\ s^{-1}$. The evolution of volume fraction martensite that formed during plastic deformation was measured with X-ray diffraction and characterized with light microscopy. Alloy 304L was found to transform readily with strain, with martensite nucleating on slip bands and at slip band intersections. Alloy 309 did not exhibit strain-induced transformation. Variations in ductility and strength with strain rate are explained in terms of the competition between hardening, from the martensitic transformation and a positive strain rate sensitivity, and softening due to deformational heating. Existing models used to predict the increase in volume fraction martensite with strain were examined and modified to fit the experimental data of this study as well as recent data for alloys 304 and 301LN obtained from the literature.

I. INTRODUCTION

AUSTENITIC stainless steels represent a large family of alloys and end uses. These steels enjoy a wide range of applications because of good corrosion resistance, good high- and low-temperature strength and ductility, and excellent weldability. The high work-hardening rate and ductility of austenitic stainless steels in the annealed state allows the application of severe forming operations. Some grades are metastable and are prone to transformation from the initial face-centered-cubic austenite (γ) to body-centered-cubic martensite (α') upon plastic deformation, commonly referred to as strain-induced martensite. Stability is mainly dependent on composition and temperature. Other factors that can affect the extent of transformation are plastic strain, strain rate, stress state, and grain size. The transformation results in increased strength, because martensite is stronger than austenite, and can, at the same time, give increased ductility if it occurs rapidly just prior to severe strain localization.

Transformation from austenite to martensite can also occur by two other means, spontaneous transformation and stress-assisted nucleation. Spontaneous transformation occurs when the material is cooled below the martensite start temperature (M_s) as occurs in conventional steels. Slightly above the M_s, stress-assisted martensite can form in response to an applied elastic stress. This type of martensitic transformation occurs until the austenite yields at a temperature designated by M_s^σ. Above M_s^σ, where the material yields by slip, new highly potent transformation sites are generated and strain-induced transformation on these new sites is possible at stresses lower than observed for the stress-assisted transformation. As temperature increases, austenite stability increases to limit the transformation. The temperature above which strain-induced martensite is not produced by plastic deformation is referred to as M_d.[1]

JOSHUA A. LICHTENFELD is with Firth Rixon-Schlosser Forge Co., Cucamonga, CA 91730. CHESTER J. VAN TYNE is with the Department of Metallurgical and Materials Engineering, Colorado School of Mines Golden, CO 80401. MARTIN C. MATAYA is with the Materials Science and Technology Division, Los Alamos National Laboratory, Los Alamos, NM 87545. Contact e-mail: mataya@lanl.gov

Manuscript submitted June 17, 2005.

The susceptibility of an alloy to strain-induced transformation depends on austenite stability, which can be roughly assessed by its martensite start temperature (M_s). Eichelman and Hull[2] studied the effect of composition on M_s and found that Cr and Ni have a moderate effect while C and N have a stronger effect on the M_s, which decreases with solute addition. The direct effect of composition on the formation of strain-induced martensite in alloy 304 was first investigated by Angel,[3] who correlated elemental compositions to the temperature at which half of the austenite is transformed by the application of 0.3 true strain in tension, denoted by M_{D30}. Again, C and N were found to have a strong effect on austenite stability. Generally, grades with less alloy content were found to be less stable. For example, 301 and 302 are less stable than 304, 305, and 309. Likewise, grades with lower C are less stable. For example, 304L and 301L are less stable than their higher carbon counterparts. Nohara *et al.*[4] modified Angel's equation to include additional elements and grain size.

It has been proposed that the transformation of austenite to martensite during plastic deformation proceeds initially as follows: austenite to ε-martensite (hcp) to α'-martensite[5,6,7] and that intersections of slip bands consisting of dense stacking fault bundles and also slip band intersections with grain boundaries and twin boundaries are potent sites for transformation. Since planar slip is integral to the transformation, the propensity for strain-induced martensite is not only a function of austenite stability but depends also on stacking fault energy (SFE), as proposed by Olson and Cohen.[1] Although it appears that the transformation may progress initially by the formation of a transitional epsilon phase, it has been shown[8,9,10] that as strain progresses, the transformation to epsilon stops and existing epsilon is completely consumed at relatively low levels of strain and that austenite transforms directly to martensite at higher levels of strain. Brooks *et al.*[11,12] showed that martensite formed directly from dislocation pileups on $\{111\}_\gamma$ slip planes in low carbon austenitic stainless steels, including 304L, without a transitional phase. Lee and Lin[13] also observed martensite growing along shear bands as well as at shear band intersections.

If the heat of deformation is retained in the workpiece and temperature increases during plastic deformation, austenite

stability increases and less martensite is formed. Bressanelli and Moskowitz[14] clearly demonstrated this effect in alloys 301 and 304 by applying various strain rates during tensile testing. They also showed that the best elongation was associated with the formation of about 50 vol pct martensite. Huang *et al.*[15] investigated 304 sheet and found a maximum in total elongation at 20 °C, a maximum in the uniform elongation (UEL) at 0 °C and a maximum in postuniform elongation at 60 °C. The uniform and postuniform maximums were correlated to the formation of a significant volume fraction of martensite before and after the onset of necking, respectively. If martensite forms well before incipient necking, then failure will result much earlier in the deformation cycle due to the lower inherent ductility of martensite phase. Peterson's[16] results from tensile tests of 301 and 304 affirmed these findings, and Tague[17] demonstrated that sheet formability is reduced if martensite forms too early or too late in the forming process.

The strain path and strain rate have been shown to affect the transformation. Hecker *et al.*[18] found that more martensite formed in 304 during balanced biaxial tension than during uniaxial tension. Murr *et al.*[19] showed that martensite formed at slip band intersections and that there were approximately two and a half times as many intersections after balanced biaxial tension compared to uniaxial tension. The density of slip bands and band intersections as well as the amount of martensite (at low strains prior to significant adiabatic heating) was found to increase with increasing strain rate.

The mechanical properties of austenitic stainless steels at moderately high strain rates have been of interest in explaining and predicting alloy behavior during forming operations. More recently, austenitic stainless steels have been considered for deployment as crash-resistant structural members in automobiles because of their good energy absorption characteristics in addition to their generally good formability. Talonen *et al.*[20] studied the effect of strain rate on tensile properties and the transformation of austenite to α'-martensite in 304 and 301LN over strain rates ranging from 3×10^{-4} to 200 s^{-1} and found that changes in the extent of martensite formation, which was highly dependent on adiabatic heating, strongly affected work-hardening rate and ultimate tensile stress (UTS).

The objective of the present study is similar to Talonen's, to investigate the effect of strain rate on the evolution of mechanical properties and strain-induced martensite during room-temperature deformation for two austenitic stainless steels, 304L and 309. The stabilities of the austenite in these two materials contrast those of Talonen's alloys and so the findings here extend the results provided by Talonen's work. Alloy 309 was selected because it is stable and so represents a good model material that provides the base property response of pure austenite. Strain rates ranging from quasi-static to high rate, 1.25×10^{-4} s^{-1} to 400 s^{-1}, are applied in tension. Both continuous tests and interrupted tensile tests, incorporating a dwell period after various levels of strain, are investigated and special attention is given to the rise in specimen temperature due to deformational heating. The proportions of the phases are monitored *via* X-ray diffraction and the morphology of the phases *via* light microscopy. An existing constitutive model for the evolution of martensite with strain is fit to measured experimental behaviors.

II. EXPERIMENTAL PROCEDURES

A. *As-Received Material*

Two grades of austenitic stainless steel, 309 and 304L, were obtained in sheet form, each with different austenite stability with respect to martensitic transformation. The steels had been commercially produced and annealed. The 304L sheet was temper rolled in the production mill after the final heat treatment. Both sheet steels had a nominal thickness of 1.5 mm (0.059 in.). Table I provides the elemental composition of the two steels. The as-received materials exhibit equiaxed grains with straight-sided annealing twins and ASTM grain sizes of approximately 7.1 and 7.5 for 309 and 304L, respectively. Table II gives the calculated M_S[2] and M_{D30}[3,4] temperatures, and stacking fault energy (SFE)[21] for the two alloys studied here as well as two from Talonen *et al.*[20]

The as-received materials were examined with X-ray diffraction to evaluate the initial volume fraction of phases in the starting microstructure. Alloy 309 was fully austenitic; however, 304L showed a significant amount (approximately 0.15 volume fraction) of α'-martensite on the as-rolled surface, attributable to temper rolling. A small amount of ε-martensite was also detected on the as-rolled surface. Samples of 304L were then chemically etched to remove the surface material. Removal of about 1 pct of the sheet thickness (0.015 mm) reduced the measured volume fraction of α'-martensite on the sheet surface to the range of 0 to 0.01, demonstrating that the high martensite condition exists only as a very thin layer on the sheet surface.

Chemical banding is typical in commercial alloys. A microscale chemical analysis was conducted from sheet surface to center to determine macroscopic and microscopic elemental segregation in 304L. The analysis was conducted on a tensile specimen, strained to 10 pct at 1.25×10^{-4} s^{-1}, with a JEOL* 840 scanning electron microscope and Geller (Geller Microanalytical Laboratory, Inc., Topsfield, MA) microscopy analysis system operating at 15 kV and 20 nA. Measurement continued until a sigma of 0.5 was achieved or a maximum of 100 seconds was reached. A standard ZAF

*JEOL is a trademark of Japan Electron Optics Ltd., Tokyo.

Table I. Composition of 304L and 309 Austenitic Stainless Steel (Mass Percent)

Type	C	Cr	Ni	P	Si	Co	N	Mn	Cu
309	0.054	22.08	12.09	0.029	0.32	0.15	0.120	1.91	0.35
304L	0.028	18.13	8.32	0.025	0.45	0.10	0.044	1.32	0.26
Type	V	Mo	Nb	Ti	Al	S	W	Fe	
309	0.06	0.21	0.02	0.01	0.01	0.008	0.02	base	
304L	0.04	0.15	0.015	<0.01	0.01	0.005	<0.01	base	

Table II. Martensite Transformation Temperatures and Stacking Fault Energy for 309 and 304L and for the Alloys from Talonen,[20] 301LN, and 304

Transformation Temperatures (°C)	Reference	309	304L	301LN	304
M_s	Eichelman and Hull[2]	*	−135	−87	−173
M_{D30}	Angel[3]	−107	35	37	20
M_{D30}	Nohara *et al.*[4]	−216	2	40	−10
Stacking fault energy (mJ/m^2)	Schramm and Reed[21]	45	17	7	18

*Temperature below absolute zero.

correction was applied. Measurements were compared to elemental standards.

B. *Tensile Testing*

To assess the effect of strain rate on the properties, tensile specimens of 309 and 304L were taken in the rolling direction from the as-received sheet and strained to fracture at ambient temperature (24 °C ± 1 °C). The tensile specimen gage section was nominally 31.75-mm long × 5.08-mm wide × as-received sheet thickness. Specimen ends were 15.24-mm wide. Overall specimen length was 152.4 mm. Strain rates of 1.25×10^{-4} s^{-1} to 1.25 s^{-1} were applied using a standard MTS servohydraulic 10 kip system with computer control. Strains were measured with an extensometer capable of measuring 100 pct engineering strain. Test rates of 10, 100, and 400 s^{-1} were applied with a MTS 810 high rate servohydraulic system equipped with a 50 kN actuator, a 500 kN frame, and a 400 gpm servovalve supplied by a 5 gallon capacity oil accumulator. The specified peak velocity is 13.5 m/s at zero load and 10 m/s at 50 pct of peak load capacity. Special low mass titanium grips were used to minimize ringing of the load cell output. Load was measured with a 40 kN capacity Kistler type 9071A piezoelectric load washer, a Kistler model 5010B amplifier (Kistler Instrument Corp., Amherst, NY) and a National Instrument BNC-2090 12-bit acquisition board (National Instrument Corp., Austin, TX). The acquisition board allowed four channels of data to be collected during the high strain rate tests: displacement, load, and two strain signals. The high rate tests were conducted in displacement control because the response time of standard extensometry is not fast enough to run the test in closed-loop control. Strain gages (Vishay Measurement Group EP-08-250BG-120 [Vishay InterTechnology Inc., Malvern, PA]) were applied to the middle of the gage section with a high-elongation adhesive (Vishay Measurements Group Epoxy Resin and Hardener A-12). Typically, the strain gage debonded after elongations in the 8 to 18 pct range. Because the actuator velocity was essentially constant, strains after debonding were calculated based on time.

The load washer data characteristics varied with strain rate. At strain rates of 10 s^{-1} (and lower), the load data did not require any filtering or post-test processing, but at higher strain rates, anomalous fluctuations were observed, commonly referred to as "ringing," and smoothing of the data was required. The 0.2 pct offset yield stress was obtained graphically from the resulting engineering stress-strain curve. Uniform elongation was obtained by determining the strain corresponding to the UTS.

To determine the evolution of martensite during deformation, tests were stopped at 5 pct. increments in strain up to the UTS. Strain rates of 1.25×10^{-4} s^{-1}, 0.125 s^{-1}, and 100 s^{-1} were employed. The volume fraction of each phase was measured by X-ray diffraction, which is described in more detail in Section IIIC. For strain rates of 1.25×10^{-4} s^{-1} and 0.125 s^{-1}, the tests were conducted on the 10 kip test system. Since the inertia of the tests at 100 s^{-1} was too great to stop the test at precise strain levels, a procedure was developed to obtain the desired conditions. Through-thickness notches, perpendicular to the tensile axis, were cut with a diamond blade into one end of the gage length in order to induce fracture at strains less than would have normally been achieved during a continuous test. Notch depth was varied to induce varying amounts of uniform strain in the major part of the gage section.

C. *Interrupted Tensile Testing*

To examine the effect of dwell periods in the application of strain, such as those experienced in sequential forming operations, or between final forming and subsequent deformation that might be encountered in service, interrupted tensile tests were conducted at constant engineering strain rates of 1.25×10^{-4} s^{-1} and 0.125 s^{-1}. The strain rates of both initial and final deformation steps were equivalent. Specimens were deformed to various strain levels in a first step and then fully unloaded, held for 15 minutes at ambient temperature, and restrained to fracture in a second step. Selected samples were evaluated for phase volume fraction with X-ray diffraction.

D. *Temperature Calculations*

The change in temperature, due to deformational heating, was calculated for tests conducted with applied strain rates of 0.125 s^{-1} and 100 s^{-1}. For frictionless deformation processes, such as tensile tests, the increase in temperature can be calculated by the following equation:

$$\Delta T = \beta \frac{\int_0^{\varepsilon_f} \sigma_{\text{ave}}\, d\varepsilon}{\rho C_p} \qquad [1]$$

where ε_f is final strain, σ_{ave} is the average stress in each strain increment determined by the trapezoid rule, ρ is the density of the steel (8.03 and 9.01 g/cm^3 for 304L and 309, respectively), C_p is specific heat (0.5 J/g °C for both alloys), and β is the fraction of deformational work that is converted to heat, assumed here to be 0.95.

The increase in temperature can be determined by Eq. [1] if adiabatic conditions are satisfied. A number of tensile tests were performed at various strain rates with thermocouples welded to the gage section of the tensile specimen. At the lowest strain rates, the calculated temperature overestimated the actual. As strain rate was increased, the calculated results eventually matched the measured. This occurred at a strain rate of 0.125 s^{-1}. Thus, it is assumed in this study that an adiabatic condition exists in the strain rate realm of 0.125 s^{-1} and greater. For adiabatic conditions, the calculated and measured temperature values were in reasonable agreement, within 5 °C. The measured values were consistently higher than the calculated values.

E. *Quantitative Estimation of Phase Fractions*

X-ray diffraction was used to perform a quantitative measurement of the volume percent of each phase for a number of deformation conditions. A small rectangular section was cut from the gage length of the tensile specimens and acid thinned to remove approximately 0.23 mm from the surface to be X-rayed. Acid thinning was performed to remove any effect of the martensite existing on the as-received sheet surface. Samples were acid thinned, rather than being thinned by mechanical methods, in order to avoid stimulation of the deformation-induced transformation. The acid employed was a solution of hydrochloric acid, nitric acid, and distilled water in 1:1:1 proportion.

X-ray diffraction analysis was conducted using Cu K_α radiation with a step time of 1 second and a step size of 0.02 deg. Diffraction was conducted with a PHILIPS* X'Pert Pro X-ray diffraction system to generate the diffraction, a PHILIPS X'Pert Data Collector to record the data, and PHILIPS Profile Fit 1.0 software to analyze the diffraction peaks. When only the austenite and α'-martensite phases were present, the ASTM method[22] was used to calculate the volume fraction of each phase. For the analysis of the as-received 304L condition, the only condition that showed some ε-martensite, the method developed by De *et al.*[10] was used. The phases were quantified by using two diffracting planes from each phase: $(200)_\gamma$ and $(311)_\gamma$ for austenite, $(200)_{\alpha'}$ and $(211)_{\alpha'}$ for α'-martensite, and $(101)_\varepsilon$ and $(102)_\varepsilon$ for ε-martensite. The depth of X-ray penetration is about 4 μm (using the calculation for pure iron).[23]

*PHILIPS is a trademark of PANalytical B.V., 7600AA Almelo, The Netherlands.

F. *Microscopy*

Microstructures were viewed on the short-transverse plane. Strained samples of 304L were tint etched to reveal the α'-martensite. The etchant was composed of two solutions that were mixed in 1:1 ratio: 0.15 g sodium-metabisulfate in 100 mL distilled water and 10 mL hydrochloric acid in 100 mL distilled water. The samples were immersed for 10 to 12 seconds and dried with forced air.

III. RESULTS AND DISCUSSION

A. *Mechanical Properties*

1. *Strengthening*

The stress-strain curves for 309 and 304L are presented in Figures 1 and 2, and values for the yield stress, UTS, and UEL are summarized in Tables III and IV, respectively. Figure 1 shows that the flow stress of 309 increases monotonically with increasing strain rate. Figure 2 shows that 304L exhibits a similar behavior at low strains; however, the trend is reversed at higher strain levels where the lowest rates give the highest strengths. At low strain rate, self-heating of the tensile specimen does not occur and the transformation of austenite to the stronger martensite proceeds uninhibited. However, when heating does occur at higher strain rate, austenite stability increases, which inhibits the transformation. In addition, SFE increases with temperature, which reduces the density of planar slip features, *e.g.*, stacking faults, slip bands, and slip band intersections, all of which have been associated with the nucleation of martensite.

The stress-strain curve for 304L at $1.25 \times 10^{-4}\ s^{-1}$, emboldened curve in Figure 2, displays a sigmoidal shape with an

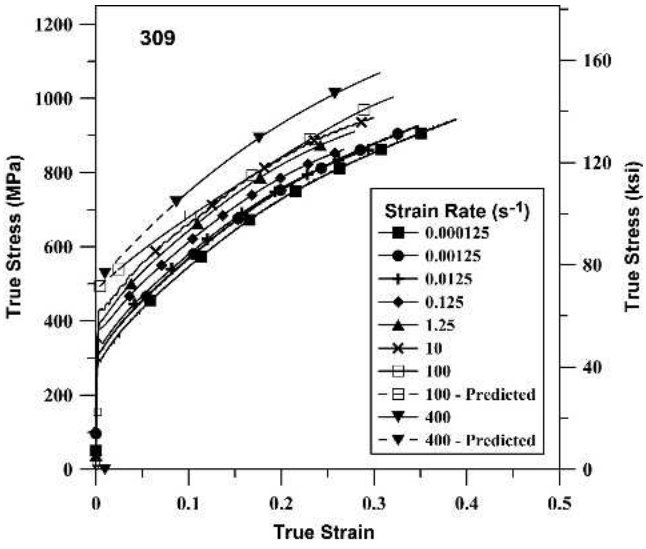

Fig. 1—True stress *vs* true strain for alloy 309 in tension at 24 °C.

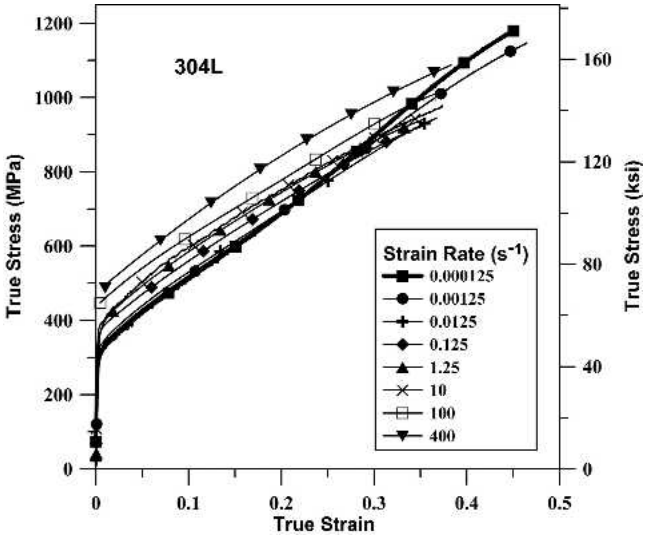

Fig. 2—True stress *vs* true strain for alloy 304L in tension at 24 °C.

Table III. Tensile Properties of 309 (Average of Three Tests)

Strain Rate (s^{-1})	0.2 Pct. Yield Stress (MPa)	Ultimate Stress (MPa)	UEL (Pct)
0.000125	291 ± 0	639 ± 1	47.9 ± 0.6
0.00125	311 ± 3	653 ± 4	42.0 ± 0.4
0.0125	343 ± 2	644 ± 3	32.5 ± 0.3
0.125	373 ± 2	659 ± 2	31.0 ± 0.4
1.25	393 ± 2	684 ± 5	31.7 ± 0.3
10	426 ± 8	703 ± 7	35.6 ± 0.6
100	492 ± 3	732 ± 2	37.1 ± 1.0
400	541 ± 20	791 ± 8	35.2 ± 0.6

Table IV. Tensile Properties of 304L (Average of Three Tests)

Strain Rate (s^{-1})	0.2 Pct. Yield Stress (MPa)	Ultimate Stress (MPa)	UEL (Pct)
0.000125	300 ± 3	755 ± 0	59.1 ± 0.7
0.00125	307 ± 5	714 ± 8	59.4 ± 0.6
0.0125	328 ± 2	654 ± 5	44.2 ± 0.8
0.125	351 ± 0	646 ± 2	42.1 ± 0.3
1.25	361 ± 5	658 ± 4	42.7 ± 0.4
10	382 ± 6	673 ± 1	45.7 ± 0.4
100	438 ± 11	699 ± 1	45.5 ± 0.6
400	480 ± 11	738 ± 4	45.9 ± 0.9

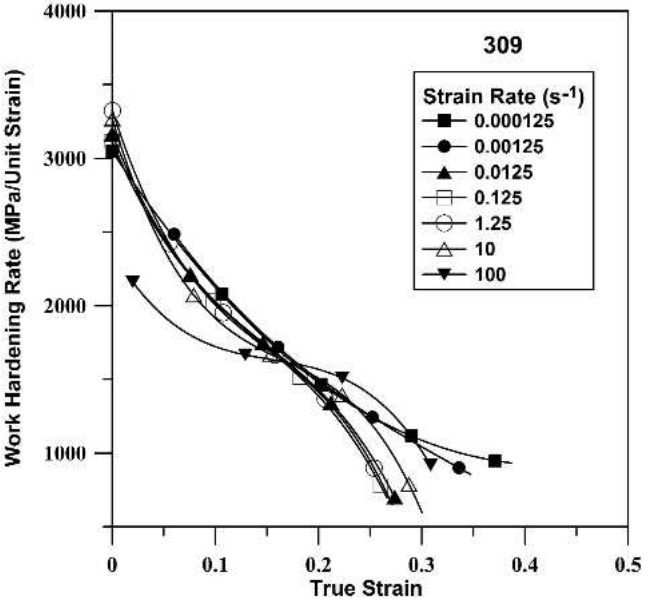

Fig. 3—Variation of work-hardening rate with true strain for 309.

apparent increase in the work-hardening rate in the midstrain realm due to the transformation to martensite. Huang *et al.*[15] studied the differential effect of martensite by evaluating the work-hardening rate. Figures 3 and 4 show the work-hardening rate as a function of strain and strain rate for 309 and 304L, respectively. Figure 3 shows that the work-hardening rates of 309 are similar for the various strain rates at low strain. At high strains, the work-hardening rate first decreases as strain rate is increased and then increases, although the changes are not great. The trend is due to increased retention of the heat of deformation as the strain rate increases from 1.25×10^{-4} s^{-1} to 0.125 s^{-1}. At higher rates, an adiabatic condition exists, so softening from increased heat retention with increased strain rate, observed in the low strain rate realm, less than 0.125 s^{-1}, plays less of a role in the high strain rate realm, greater than 0.125 s^{-1}. Some additional heating occurs in the high rate realm as a result of the increased flow stress encountered as rate is increased. The observed hardening with increasing strain rate ensues because there is progressively less time for thermally activated plastic flow.

In comparison, the work-hardening behavior of 304L (Figure 4) in the high strain realm is generally greater than 309. This is due to the formation of strain-induced martensite in

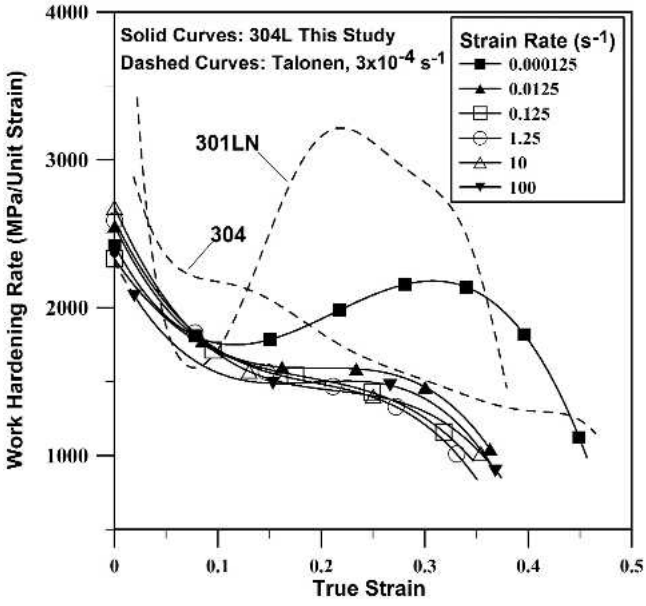

Fig. 4—Variation of work-hardening rate with true strain for 304L and also for 304 and 301LN from Talonen.[20]

304L at every strain rate, albeit, little forms at the highest strain rates because of significant specimen heating, as shown in Section IIID. In addition, 304L has a lower SFE and will exhibit more planar slip, which also results in increased work-hardening rate. Notable in Figure 4 is the extreme secondary hardening at the lowest strain rate, beginning at a strain of about 0.1. The secondary hardening gives rise to the sigmoidal behavior of the stress-strain curve in Figure 2. Huang[15] associated the minimum in the work-hardening rate curve with the onset of the strain-induced transformation. At this strain rate, specimen heating does not occur and the phase transformation operates unhindered, once initiated. Also plotted in Figure 4 are the data from Talonen *et al.*[20] for 301LN and 304, which was tested in tension at 3×10^{-4} s^{-1}. The two behaviors span that of 304L, tested at 1.25×10^{-4} s^{-1}. After a critical amount of strain, about 0.07, the work-hardening rate of 301LN increases rapidly with strain and achieves a significantly higher value compared to the behavior of 304L. Alloy 304 shows less hardening and according to Talonen forms a relatively small amount of martensite. The amount of secondary hardening for the four alloys correlates directly with the volume fraction of strain-induced martensite. For example, after 0.3 strain at 24 °C, 301LN forms the most martensite, 80 vol pct, followed by 304L with 34 vol pct, 304 with 11 vol pct, and finally 309 with no martensite. This alloy ranking, from least to most stable, is consistent with the calculated M_{D30} temperatures from Nohara,[4] shown in Table II, which are 40 °C, 2 °C, −10 °C, and −216 °C, respectively, for the four alloys. The SFE (Table II) for the four shows an equivalent ranking, 7, 17, 18, and 45 mJ/m^2, respectively, with lower SFE associated with lower stability.

Figure 5 and Tables III and IV show the variation of yield strength and UTS with strain rate for 309 and 304L. Yield strength for both alloys increases moderately with strain rate, which is consistent with a positive strain rate sensitivity. As strain rate increases, the UTS of 309 does not vary much in

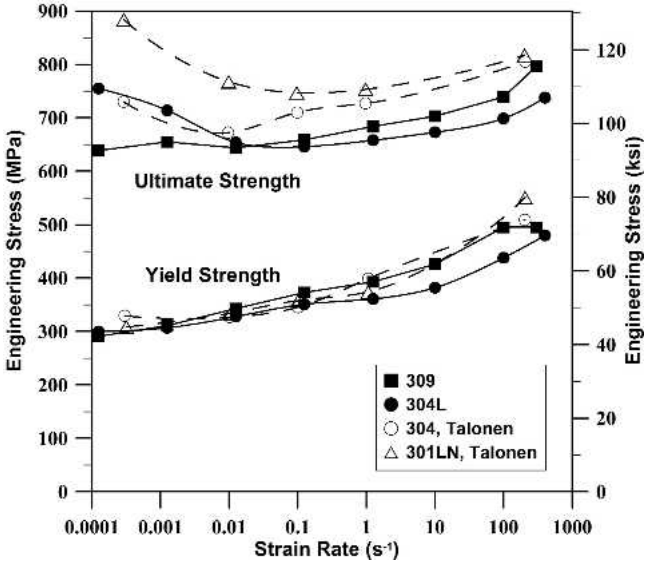

Fig. 5—Variation of 0.2 pct offset yield strength and UTS with strain rate for 309 and 304L, and also for 304 and 301LN from Talonen.[20]

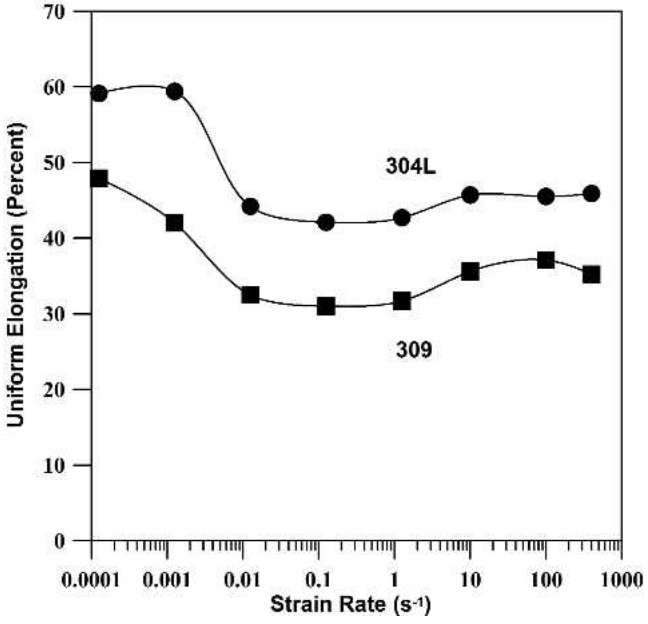

Fig. 6—Variation of UEL for 309 and 304L with strain rate.

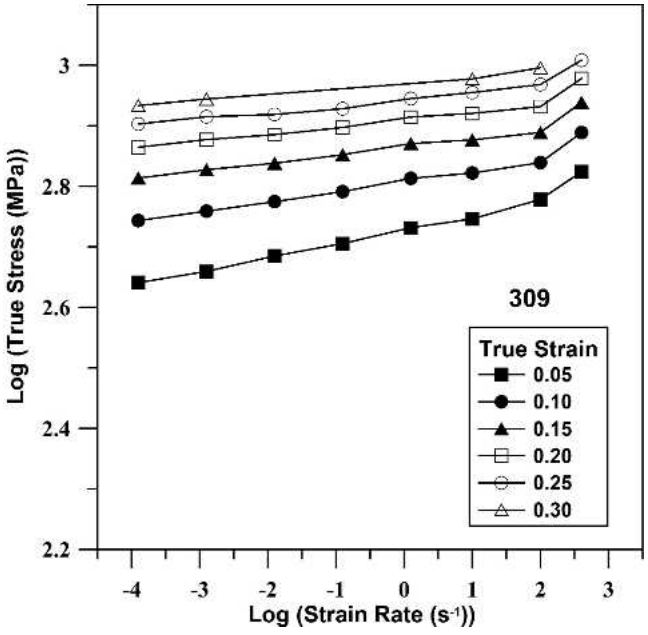

Fig. 7—Variation of log true stress with log strain rate for 309.

the low rate regime, then increases up to a strain rate of 10 s^{-1} and subsequently increases more rapidly with increasing strain rate. The UTS does not increase in the low rate regime because the increase due to strain rate sensitivity is moderated by increased deformational heating with increased strain rate.

In contrast, alloy 304L exhibits the greatest UTS at the lowest strain rate and exhibits a minimum at approximately 0.125 s^{-1}. The decrease in UTS for 304L occurs because as strain rate increases more of the heat from deformation is retained in the sample. At a strain rate of 1.25×10^{-4} s^{-1}, there is no temperature rise. The test is essentially isothermal. As rate increases, more heat is retained and the tensile test becomes adiabatic at approximately 0.125 s^{-1}. Since martensite is the stronger phase, a reduction in the volume fraction due to specimen temperature rise produces a corresponding reduction in strength. At strain rates greater than 0.125 s^{-1}, additional heating occurs due to the increase in flow stress, from Eq. [1], and transformation is inhibited further. The density of nucleation sites for the transformation has been observed to increase with strain rate,[19] which would act to counter the effect of additional heating. A moderate increase in UTS with increase in strain rate is observed. In comparison, 309 shows more strengthening with strain rate, in the high strain rate realm. Alloy 309 is not subject to the loss of martensite as specimen temperature increases.

Data for 304 and 301LN from Talonen *et al.*[20] are also plotted in Figure 5. The trends in UTS for each are similar to 304L, a decrease in UTS with increasing strain rate in the low strain rate regime due to the suppression of the transformation by test specimen self-heating, followed by moderate increases at higher strain rates.

2. *Ductility*

Figure 6 shows the variation in UEL with strain rate for 304L and 309. Similar to the variation in UTS, UEL of 304L is greatest at low strain rate and then decreases as strain rate increases to 0.125 s^{-1}. Like UTS, loss of UEL is attributed to increased specimen heating and a concomitant loss in work hardenability of austensite as well as to a loss in the amount of strain-induced martensite. Alloy 309 shows a similar loss, presumed to be solely due to a loss in work hardenability. To verify the stability of 309, multiple specimens were strained isothermally, at 24 °C to 0.3 strain at 1.25×10^{-4} s^{-1}, and analyzed with X-ray diffraction. Martensite was not observed.

At higher strain rates, where deformation is essentially adiabatic and specimen temperature does not increase significantly with strain rate, UEL increases with strain rate due at least in part to increasing strain rate sensitivity, *m*. Similar trends in ductility and strength observed here for 309 have been seen in other stable austenitic stainless steels.[24,25]

3. *Strain rate sensitivity*

Figures 7 and 8 show the variation in log stress *vs* log strain rate at various levels of strain for 309 and 304L, respec-

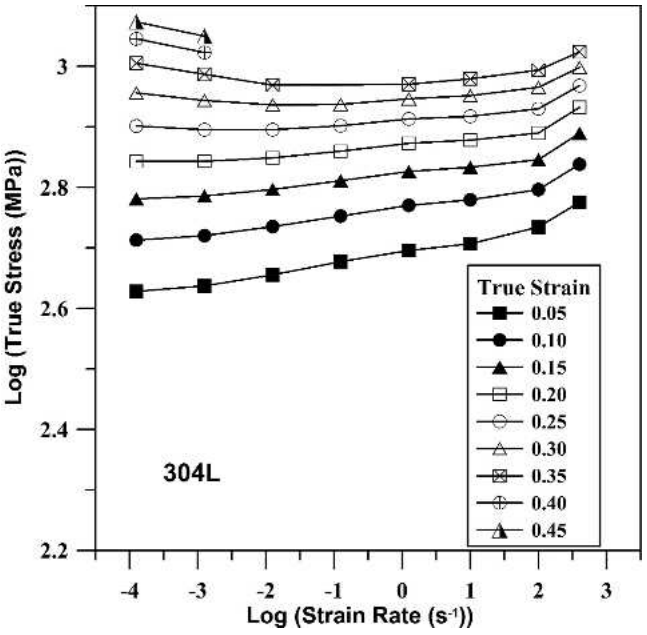

Fig. 8—Variation of log true stress with log strain rate for 304L.

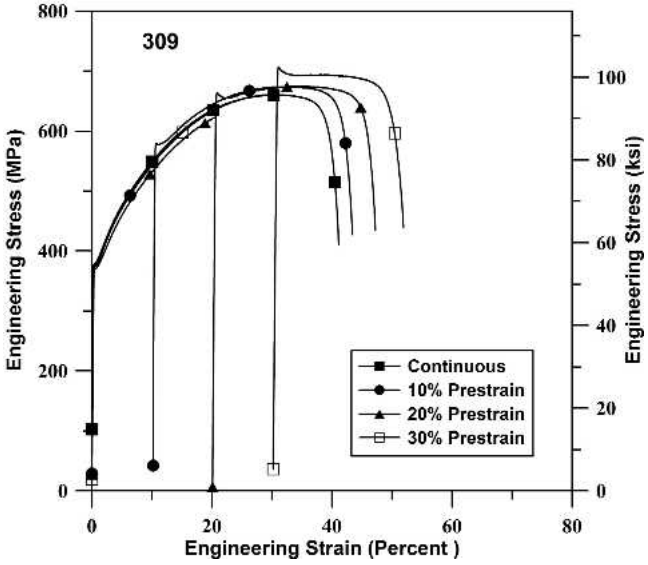

Fig. 9—Engineering stress-strain behavior of 309 for various increments of prestrain, applied in a first step, followed by unloading, a 15-min dwell period, and reloading to failure in a second step.

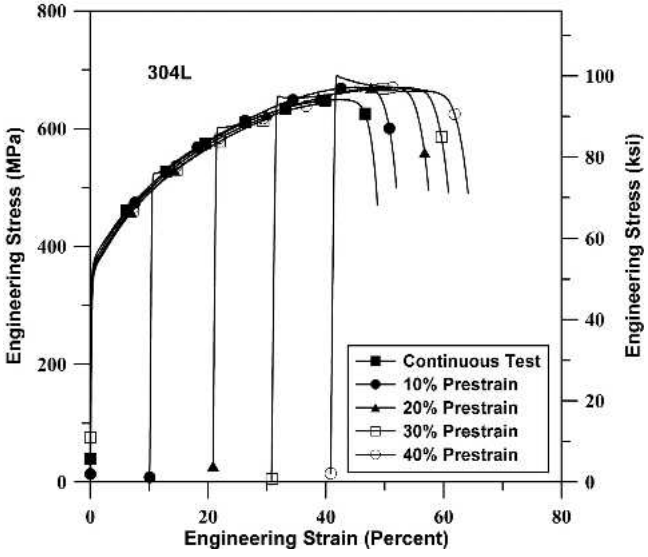

Fig. 10—Engineering stress-strain behavior of 304L for various increments of prestrain, applied in a first step, followed by unloading, a 15-min dwell period, and reloading to failure in a second step.

tively. The slope of these curves represents the strain rate sensitivity. For 309, the slope is positive and constant over the strain rate range tested up to 100 s^{-1} and independent of strain level. For 304L, the slope is nearly constant in the low strain rate low strain realm; however, at strain levels above 0.25, a negative strain rate sensitivity is observed, which is consistent with a loss of capacity to transform to the stronger martensite phase as specimen self-heating increases. The reduction in strain rate sensitivity is consistent with the previously described reductions in UTS and UEL with increasing strain rate in the low strain rate regime, which are also due to the specimen self-heating phenomenon. Measurements showing a reduction in strain-induced martensite with increasing strain rate are presented in Section IIIC and IIID.

A sharp increase in sensitivity occurs above 100 s^{-1} for both materials. Stout and Follansbee[26] also observed an increase in flow stress above 100 s^{-1} for a 304L, while Lee and Lin[27] saw a similar increase for 304L, but above 1000 s^{-1}. A pronounced increase in strength at high strain rates has also been observed in other fcc metals such as aluminum[28,29] and copper.[30,31]

B. *Interrupted Tensile Tests*

Figures 9 and 10 and Tables V and VI show the results of interrupted tensile tests conducted at strain rates of 1.25×10^{-4} s^{-1} and 0.125 s^{-1} for 309 and 304L, respectively. The values of UTS and UEL of tensile specimens pulled to failure at the lowest strain rate are not affected by inserting an unloading step with a 15-minute dwell period after an initial strain of 30 pct. For example, the UTS and UEL values for 309 (Table V) are 639 and 644 MPa and 47.6 and 48.7 pct, respectively. The UTS and UEL values for 304L (Table VI) are 755 and 748 MPa and 67.8 and 68.8 pct, respectively. At the higher strain rate, 0.125 s^{-1}, both UTS and UEL increase with an intermediate unloading step and a 15-minute hold prior to restraining in a second step. For example, Table V shows that the UEL of 309 increases from 31.6, for a continuous test, to 32.4, 34.2, and 38.2 for first-step strain levels of 10, 20, and 30 pct engineering strain, respectively. Likewise, the UEL in 304L (Table VI) increases from 42.1, for a

Table V. Tensile Properties of 309 for Continuous and Interrupted Tensile Tests

Strain Rate (s^{-1})	First-Step Strain (Pct)	Ultimate Stress (MPa)	UEL (Pct)
0.000125	0	639 ± 1	47.6 ± 0.6
0.000125	30	644 ± 3	48.7 ± 0.3
0.125	0	659 ± 2	31.6 ± 0.6
0.125	10	671 ± 2	32.4 ± 0.8
0.125	20	684 ± 1	34.2 ± 0.4
0.125	30	694 ± 1	38.2 ± 0.5

Table VI. Tensile Properties of 304L for Continuous and Interrupted Tensile Tests

Strain Rate (s^{-1})	First-Step Strain (Pct)	Ultimate Stress (MPa)	UEL (Pct)	Vol Pct α'-Martensite
0.000125	0	755 ± 0	59.1 ± 0.7	67.8
0.000125	30	748 ± 3	59.5 ± 0.8	68.8
0.125	0	646 ± 2	42.1 ± 0.3	9.4
0.125	10	672 ± 2	45.2 ± 0.5	20.2
0.125	20	676 ± 6	49.3 ± 1.2	20.1
0.125	30	668 ± 4	53.5 ± 0.2	19.9

continuous test, to 45.2, 49.3, and 53.5 pct for initial strain levels of 10, 20, and 30 pct. Generally, the UTS also increases progressively with the strain applied during the first step.

Figures 9 and 10 show that, in addition to a general increase in the flow stress curve upon reloading, a yield point is also generated upon reloading. The appearance of a yield point might be considered the result of strain aging of the dislocated structure during the 15-minute dwell period prior to reloading. In fact, Talonen *et al.*[32] and Rathburn *et al.*[33] have recently demonstrated that significant strain aging occurred in annealed and tensile-prestrained 301 and cold-rolled 301, respectively. Assuming the activation energy reported by Rathburn for the diffusion of carbon to dislocations in martensite in cold-rolled 301, 14 kJ/mole, a 5 pct increase in strength might be anticipated for the 304L in this study after about 45 minutes at 24 °C.

In both of the preceding studies, strain aging occurred only if strain-induced martensite was present after deformation and prior to the strain aging heat treatment. In the former study, strain aging was not observed in 304 after 15 pct prestrain in tension and a subsequent 400-minute age at 170 °C, presumably due to the small amount of martensite present (0.3 vol pct). In the latter study, alloy 305 was prestrained 20 pct in tension at −25 °C and aged for 30 minutes at temperatures ranging from 25 °C to 600 °C. Martensite was not formed during prestraining nor was strain aging detected.

Based on the appearance of an apparent strengthening in the 309 alloy in this study, which like 305 is stable upon deformation at room temperature, it is apparent that strain aging is not a major contributor to the apparent strengthening in 309. Because 304L shows nearly equivalent strengthening to that observed for 309, strain aging does not appear to be operative in 304L. The apparent increase in the flow curve upon reloading is attributed solely to the softening that occurs during prestraining as a result of the heat of deformation. Heat is dissipated during the dwell, and upon reloading, a higher flow stress is observed, compared to that observed just prior to unloading.

The appearance of a yield point is determined to be an artifact of testing. The actuator velocity was examined in detail and it was determined that the applied strain rate during a short period of time upon reloading was anomalously high, about twice as high in the vicinity of the yield point as that encountered immediately after the yield point and during the remainder of the test. Due to the temporary loss of closed loop control because of the relatively high applied strain rate, 0.125 s^{-1}, an apparent yield point was generated.

In summary, strain aging was not observed. However, strengthening is observed because of the interruption in strain and is due to the dissipation of the heat of deformation during the dwell period. Both UTS and UEL are observed to increase as a result of moderating the temperature increase.

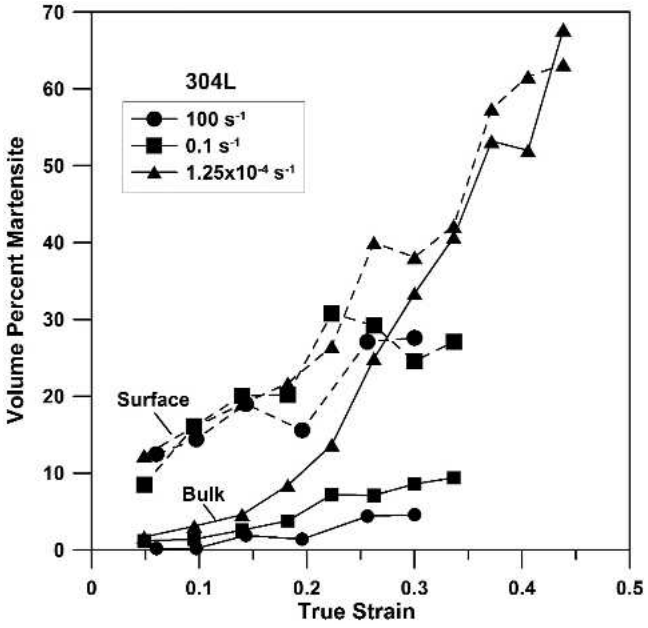

Fig. 11—Variation in volume percent α'-martensite with true strain for surface and bulk material for three strain rates.

C. *Evolution of Martensite*

1. *X-ray diffraction measurements*

Interrupted tests for strain rates of 1.25×10^{-4} s^{-1}, 0.125 s^{-1}, and 100 s^{-1} were performed and X-ray diffraction was used to measure the evolution of martensite in both the bulk and the surface material. Figure 11 shows the change in volume percent martensite with strain for the bulk material (below sheet surface). Epsilon-martensite was not detected in any of the bulk measurements. The tests strained at the lowest rate exhibited a significantly greater amount of α'-martensite than the two higher rates. For example, after a strain of 0.3, the volume fraction of α' at the low rate was about 0.34 compared to 0.09 to 0.05 for strain rates of 0.125 s^{-1} to 100 s^{-1}, respectively. Heat generated in the specimen inhibits martensite formation. At the lowest strain rate, the rate of martensite formation with strain is initially low, but above about 0.17 strain, the rate increases substantially. For the two higher strain rates, 0.125 s^{-1} and 100 s^{-1}, the rate of martensite formation is relatively low at all levels of strain. Because the temperature increase was greater during the 100 s^{-1} test, due to the overall higher flow stress, less martensite formed compared to the 0.125 s^{-1} test.

Figure 11 also shows the evolution of martensite on the sheet surface. At low strains, the high level of martensite on the as-received surface is maintained. As strain is increased further, the rate of martensite formation is actually higher than in the bulk. This is due to the prior amount of work that was imparted to the surface during temper rolling. In essence, the surface material is in an accelerated transformation period compared to the bulk material, which is well annealed and does not experience accelerated transformation until a strain of about 0.17 is achieved. At the lowest strain rate, the martensite at the surface continues to increase but at a lower rate

compared to the bulk material so that at high strain, about 0.4, the curves coincide. In contrast, at the two higher strain rates, the surface material transforms to martensite at a moderately faster rate than the bulk material so that the difference in martensite content at the two locations increases with strain. A likely explanation is that the temperature at the surface may actually be less than that in the bulk, which would be consistent if the surface deformation were not ideally adiabatic. The surface data appear to exhibit more scatter than the bulk, possibly due to the varying amounts of martensite on the surface, from location to location, in the as-received (temper-rolled) condition.

The X-ray diffraction results indicate that ε-martensite is not present in any of the deformed conditions studied here, and therefore, the sequence of transformation is $\gamma \rightarrow \alpha'$, at least for strains greater than 0.05.

2. *Microstructure*

The microstructural evolution of martensite with strain at a strain rate of $1.25 \times 10^{-4}\ s^{-1}$ is shown in Figure 12. At

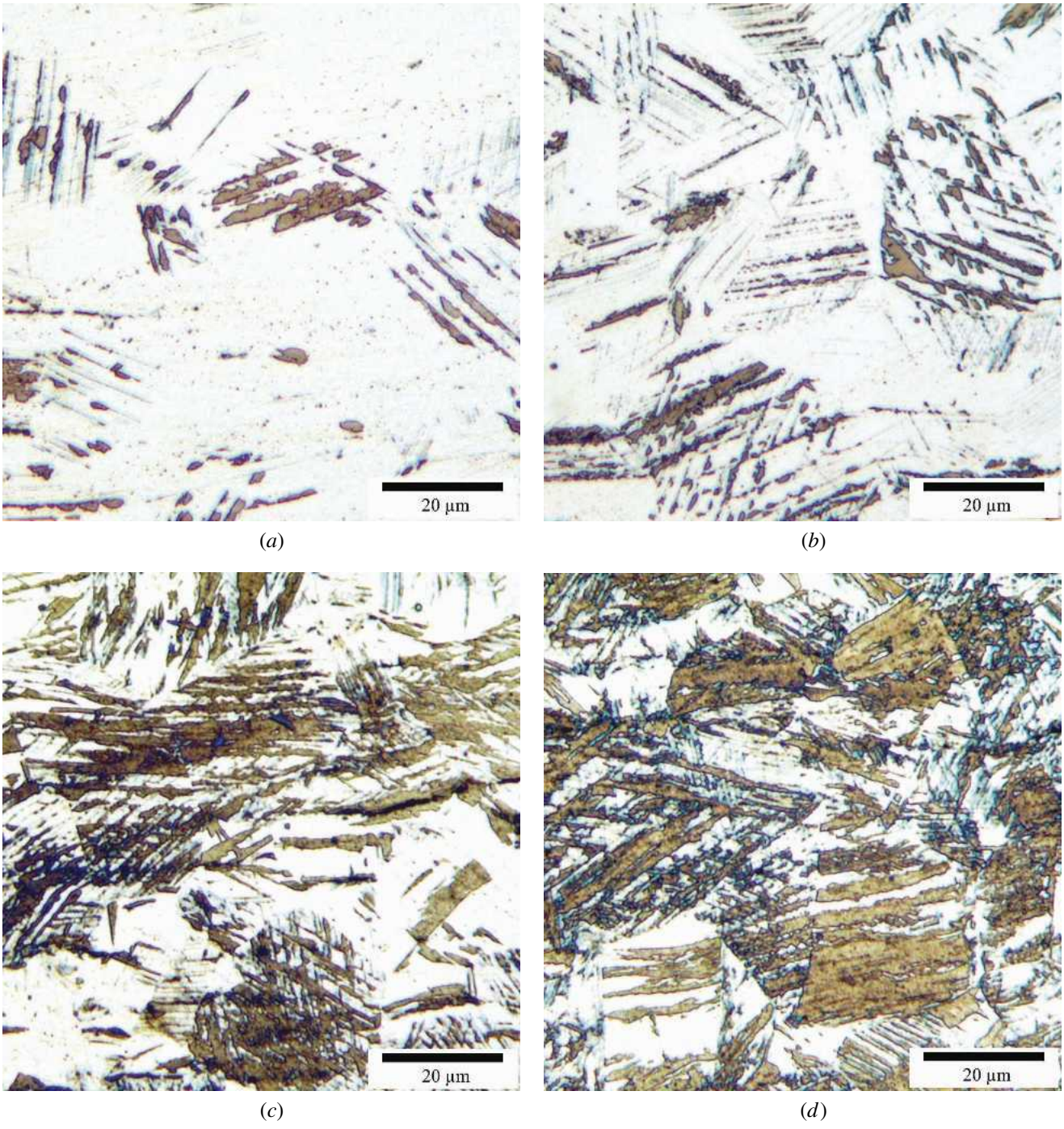

(*a*) (*b*) (*c*) (*d*)

Fig. 12—Light microscopy of 304L tension specimens deformed at a strain rate of $0.000125\ s^{-1}$ to strains of (*a*) 10 pct (3.1 vol pct α'), (*b*) 20 pct (8.1 vol pct α'), (*c*) 30 pct (24.9 vol pct α'), and (*d*) 45 pct (53.2 vol pct α'). The straw color phase is the α'-martensite and the white phase is the austenite matrix. Color tint etchant was applied.

an engineering strain of 10 pct (Figure 12(a)), the α'-martensite appears to have nucleated on shear bands. Subsequent growth of the α' from the shear bands into the unbanded adjacent matrix is shown by the rounded, advancing interfaces. Growth appears to occur preferentially to one side of the shear band. Brooks *et al.*[11,12] observed nucleation at dislocation pileups on $\{111\}_\gamma$ slip planes and subsequent growth of α' laths to one side of the slip plane and suggested that the growth occurs to the side with the missing half-planes of atoms, because the lattice there can better accommodate the extra volume of the new martensite. The habit plane of the α' growth was close to the $\{225\}_\gamma$. Murr *et al.*[19] found that α' laths are composed of many small α' embryos stacked together. They concluded that the formation of closely spaced α' embryos coalesce into continuous laths giving the appearance of propagation from an initial embryo in a $\{111\}_\gamma$ plane or out of it. Also, the number of shear band intersections increased in 304 when comparing low and high strain rate tests and the increase in temperature due to adiabatic heating resulted in an increase in SFE, which resulted in more narrow shear bands. Figure 12(b) shows that as strain increases to 20 pct, the number of shear band intersections increases and martensite is observed to form at some of the intersections, which is a common observation in the literature. After strains of 30 and 45 pct (Figures 12(c) and (d)), the nucleated martensite grows in size, consuming the original nucleation events.

Figure 13 shows a microstructural comparison of two samples that were both strained to 30 pct, one at a strain rate of $1.25 \times 10^{-4}\ s^{-1}$ having 24.9 vol pct α' and the other at $100\ s^{-1}$ having 4.4 vol pct α'. The micrograph of the $100\ s^{-1}$ sample shows that the morphology of the martensite is similar to that formed at the lower strain rate. This observation is consistent with the findings of Staudhammer *et al.*,[34] who concluded that strain rate does not affect the morphology of the α'-martensite. The fine structure, however, may be affected by strain rate. Ferreira *et al.*[35] recently observed in TEM of 304 a significantly higher density of stacking faults and deformation twins and a lower density of perfect dislocations after straining at a strain rate of 10^3 compared to $10^{-3}\ s^{-1}$. They calculated that a minimum critical shear stress value of 184 MPa would enhance the nucleation of partial dislocation loops in 304 at the expense of the nucleation of perfect dislocation loops and argued that the higher stress incurred at the high strain rate accounts for the observed increase in stacking fault and deformation twin densities. Since these features are integral to the nucleation of strain-induced martensite, one would expect more transformation as strain rate increases in the absence of specimen self-heating.

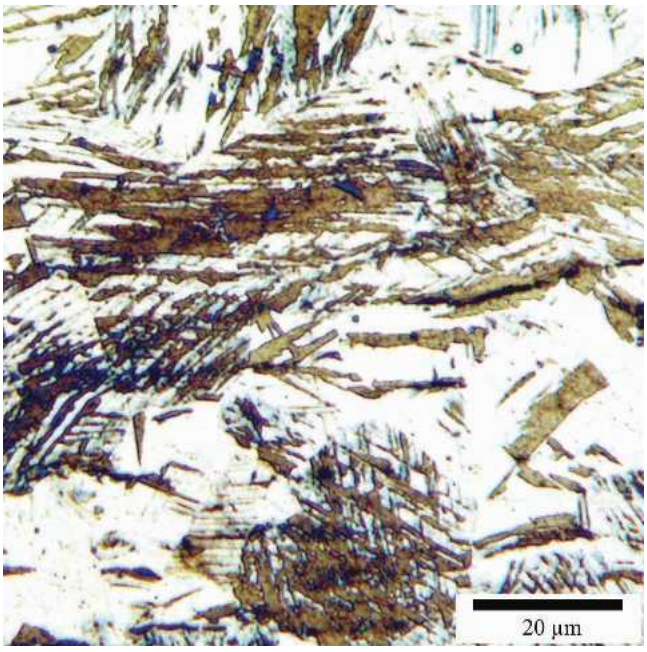

(*a*)

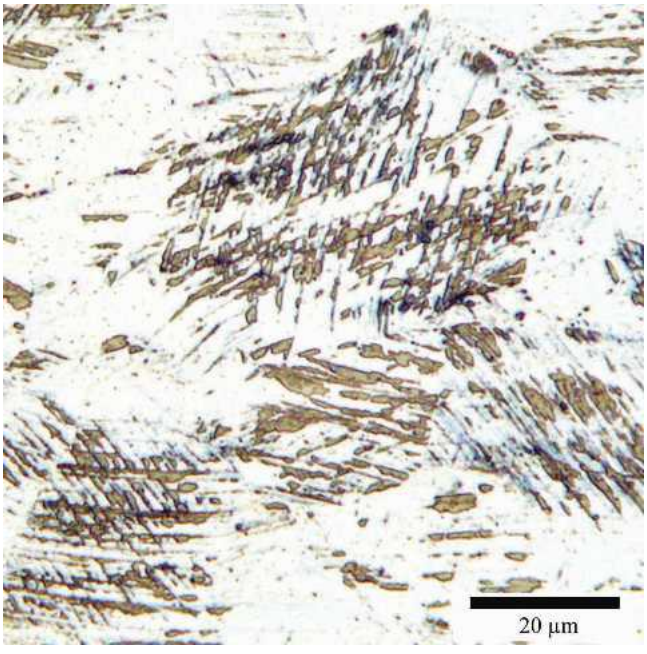

(*b*)

Fig. 13—Light microscopy of 304L tension specimens strained to 30 pct at a strain rate of (*a*) $1.25 \times 10^{-4}\ s^{-1}$ (24.9 vol pct α') and (*b*) $100\ s^{-1}$ (4.4 vol pct α'). The straw color phase is the α'-martensite and the white phase is the austenite matrix. Color tint etchant was applied.

3. *Effects of chemical segregation*

Figure 14 shows the short-range and long-range variation in Cr, Mn, and Ni determined by microprobe analysis of a tensile specimen strained 10 pct at a strain rate of $1.25 \times 10^{-4}\ s^{-1}$, viewed on the short-transverse plane. The estimated variation in M_{D30} is also shown. Short-range segregation, banding, is evident. Generally, a band with higher Cr will have lower Ni and Mn and *vice versa*. The long-range segregation, from sheet surface to midthickness, appears to be minimal; however, a slight increase in Cr and decrease in Ni and Mn near the midthickness region is noted. As a result of the segregation, the M_{D30} temperature from Nohara[4] varies in the short range by as much as 19 °C, peak to peak, which indicates a fairly significant variation in austenite stability. The variation occurs in spite of the inverse relationship between the segregation of Cr vs Ni and Mn because the coefficients for Ni and Mn in Nohara's equation are significantly greater than the coefficient for Cr. In the long range, M_{D30} is relatively constant but does increase slightly near the midthickness position starting at about 0.4 of the thickness, paralleling the changes in chemistry discussed previously.

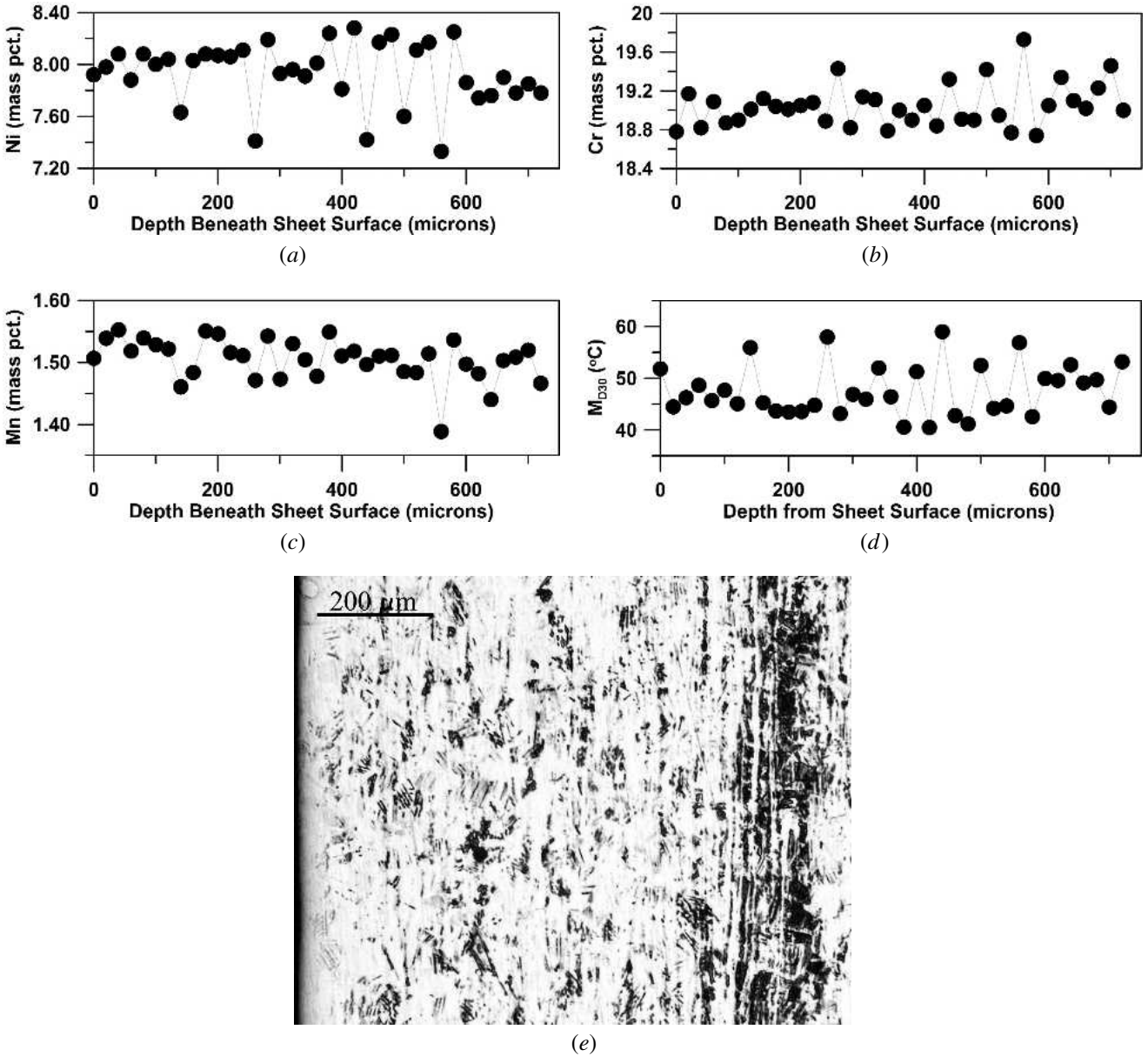

Fig. 14—Elemental segregation (*a*) Ni, (*b*) Cr, (*c*) Mn; (*d*) M_{D30}; and (*e*) microstructure of 304L strained 10 pct at $1.25 \times 10^{-4}\ s^{-1}$. In (e), sheet surface at left and sheet midplane near the right, in the vicinity of the dark vertical band. Longitudinal section.

Figure 14 also shows the etched microstructure. The sheet surface is on the left and midthickness near the right in the micrograph. The dark phase in the structure is strain-induced martensite and the light area is the austenite matrix. Thin bands of martensite are evident and are due to the short-range variations in elemental concentration, or chemical banding. The presence of banding should have minimal effect on tensile properties, but might affect crack propagation in the plane of the sheet.

D. *Transformation Models*

Sugimoto *et al.*[36] characterized the transformation of retained austenite to strain-induced α'-martensite in a TRIP-aided dual-phase steel by the following relationship:

$$\log (f_\gamma) = \log (f_{\gamma 0}) - k\varepsilon \qquad [2]$$

where f_γ is the volume fraction retained austenite, ε is true strain, $f_{\gamma 0}$ is the initial volume fraction, and k is a constant that varies with temperature. Equation [2] can be adapted for 304L, which exhibits an initially slow rate of transformation with strain below about 0.17 and more rapid transformation at higher strains, by segmenting the strain into two regimes as follows:

$$\log (f_\gamma) = \log (f_{\gamma 0}) - k_1\varepsilon_1 - k_2\varepsilon_2 \qquad [3]$$

where ε is the strain applied in tension, and the subscripts 1 and 2 refer to low and high strain ranges, using 0.17 strain as the transition strain. In the low strain range, $\varepsilon_1 = \varepsilon$ and $\varepsilon_2 = 0$. In the high strain range, $\varepsilon_1 = 0.17$ and $\varepsilon_2 = \varepsilon - 0.17$. The k constants were evaluated as a function of strain rate, and expressions for their variation with strain rate are given in Table VII. Figure 15 shows the model prediction

Table VII. Expressions for Constants in Eq. [3]; the term "SR" Denotes Strain Rate Value

Constants	Value
$f_{\gamma 0}$	100 (100 pct austenite in the bulk)
k_1	0.0015 (log (SR))^2 − 0.0151 (log (SR)) + 0.0636
k_2	−0.0082 (log (SR))^3 + 0.0351(log (SR))^2 − 0.0515 (log (SR)) + 0.1352

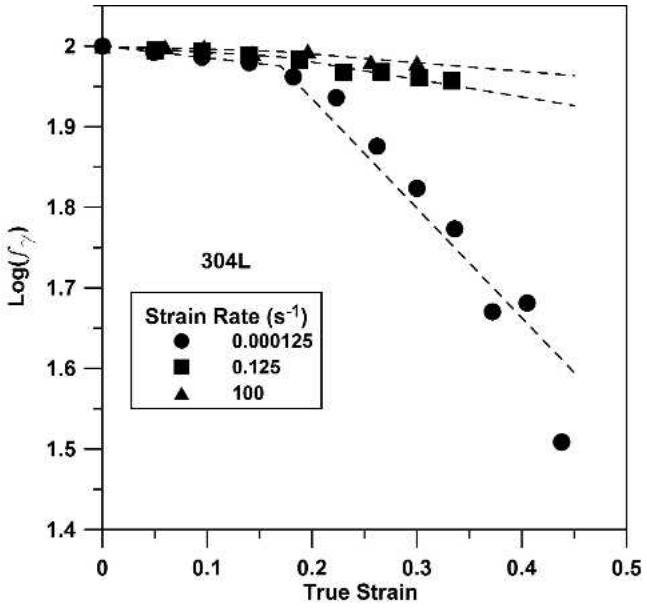

Fig. 15—Comparison of the modified Sugimoto model predictions, Eq. [3], with experimental data for 304L.

compared to the measured data. A shortcoming of this approach is that a saturation level in the volume fraction austenite is not predicted.

Olson and Cohen[1] used data from Angel[3] for alloy 304 to model the kinetics of the strain-induced transformation. The model employs two temperature-dependent constants, which are phenomenological in nature, and true strain as shown:

$$f_{\alpha'} = 1 - \exp\left\{-\beta\left[1 - \exp\left(-\alpha\varepsilon\right)\right]^{4.5}\right\} \qquad [4]$$

where $f_{\alpha'}$ is volume fraction α'-martensite; α is a strain-independent constant that represents the rate of shear-band formation, which is dependent on stacking fault energy and strain rate and potentially grain size and crystallographic texture; and β is related to the probability that an intersection will form an embryo and is temperature dependent through its relationship to the chemical driving force for the martensitic transformation. The exponent of 4.5 was determined by Olson and Cohen for Angel's 304 data and also appears to be appropriate in this study, as shown later in this section. Figures 16 and 17 show the predicted variations in α and β with temperature.

Hecker *et al.*[18] applied Olson and Cohen's model to 304 and suggested that the α and β functionality with temperature is similar to that proposed by Olson and Cohen (Figures 16 and 17). In both studies, α was assumed to

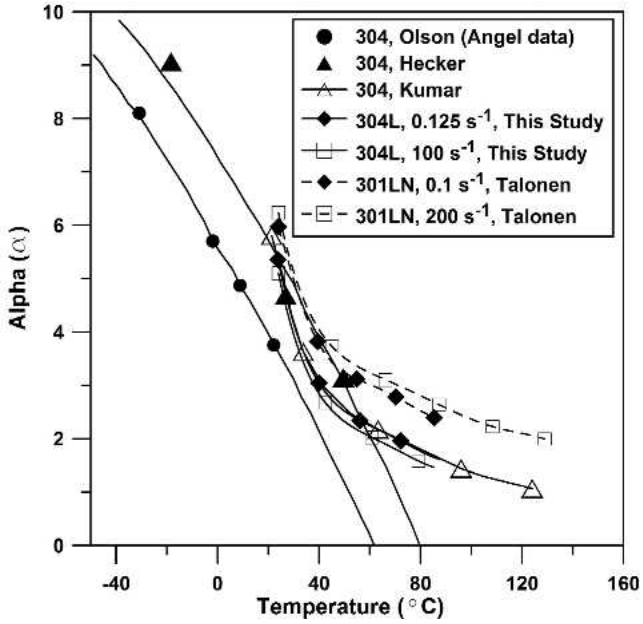

Fig. 16—Predicted variation of the coefficient alpha (Eq. [4]) with temperature and corresponding experimental data for a number of investigations.[1,18,20,37]

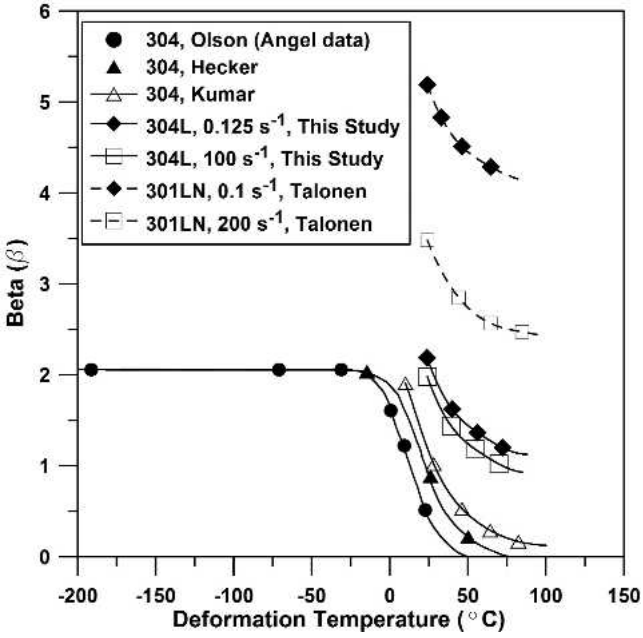

Fig. 17—Predicted variation of the coefficient beta (Eq. [4]) with temperature and corresponding experimental data for a number of investigations.[1,18,20,37]

decrease rapidly to zero and β more gradually to zero as temperature increased from 25 °C to about 75 °C. Assuming these functionalities with temperature, Eq. [4] can be successfully fit to the 304L data of the isothermal test at 1.25×10^{-4} s^{-1} (results not presented). For the adiabatic tensile test conditions that develop at higher strain rates, Eq. [4] cannot be applied directly because α and β vary during deformation due to their dependence on temperature and thus they vary with strain for adiabatic deformation. In this case, the

variation of the volume fraction martensite, $f_{\alpha'}$, with strain can be obtained by summing the increments of $f_{\alpha'}$ as strain increases while applying the instantaneous values of α and β for the average temperature of the strain increment. To facilitate the summation, Eq. [4] was differentiated with respect to strain giving the following:

$$df_{\alpha'}/d\varepsilon = 4.5\alpha\beta \exp\left(-\alpha\varepsilon - \beta\left(1 - \exp\left(-\alpha\varepsilon\right)\right)^{4.5}\right)\left(1 - \exp\left(-\alpha\varepsilon\right)\right)^{3.5} \quad [5]$$

The temperature increase during deformation was measured. For example, at 0.125 s^{-1}, temperature increased from 24 °C to 83 °C by test end and at 100 s^{-1} from 24 °C to 89 °C. The measured temperature at selected values of strain is presented in Table VIII. The transformation behavior was calculated for the adiabatic conditions assuming the general behavior of α and β with temperature, both approaching zero at about 75 °C, as suggested by Olson and Cohen, and by determining the coefficients exact functionality from the isothermal test discussed previously, without regard for a strain rate dependency. The volume fraction martensite was grossly underestimated compared to the experimental data (predicted behavior not shown). The rapid approach to zero by α between 24 °C and 75 °C and also β approaching zero in this regime was apparently responsible for the underestimation. Peterson[16] measured as much as 8 pct martensite in 304 deformed at 75 °C, and the data suggested that a finite amount of martensite may form at 100 °C, which further indicates that the suggested behavior of the coefficients with temperature is not applicable here. Further, because α is representative of SFE, which increases gradually with increasing temperature in the temperature realm of interest, one might expect that it would not approach zero abruptly but gradually. Consistent with this suggestion, Kumar and Singhal[37] studied the variation of strain and temperature along the gage length of 304 specimens tested in tension at various strain rates and showed that α approaches zero asymptotically. Both α and β have finite values well above 100 °C, as shown in Figures 16 and 17. In fact, examination of the trend indicated by the two high-temperature data points of Hecker indicates that α probably does not approach zero abruptly, as was concluded.

The behaviors found by Kumar and Singhal were subsequently assumed in this study to model the transformation behavior for the nonisothermal conditions at higher strain rates. The values of the coefficients were estimated with the least-squares analysis of the experimental data assuming zero transformation at zero strain at a starting temperature of 24 °C and assuming the coefficients decreased with temperature, as shown by Kumar and Singhal. The coefficients were analyzed separately for each strain rate, but as shown in Figures 16 and 17, the values at 24 °C varied from each other only slightly. Figure 16 shows that the value of α for 304L near 24 °C is similar to the values for 304, which is consistent with the similar SFE for the materials (Table II). The values of β are somewhat higher than 304, which would be consistent with the lesser stability of the austenite in 304L, indicated by its higher M_{D30} and lower M_s (Table II).

Also shown in Figures 16 and 17 is the behavior of the coefficients for 301LN data of Talonen *et al.*, [20] which were calculated as described previously. The values for α were moderately higher than the 304 and 304L data, which is consistent with the lower SFE (Table II). The values for β were significantly higher than the other alloys, indicating much less stability of the austenite in 301LN (as indicated by a higher M_s temperature, −87 °C, compared to the 304 of Kumar and Singhal and 304L studied here, −151 °C and −135 °C , respectively).

Figures 18 and 19 present the resulting model predictions for 304L in this study and 301LN from Talonen *et al.*, respectively. The model results are in good agreement with the experimental data. Thus, the preceding data and methodology to predict volume fraction martensite could be combined with finite-element predictions of temperature, strain, and strain rate gradients in deforming components, such as in structural automotive members undergoing crash scenarios, to predict the local evolution of martensite, strength, and energy absorption.

Table VIII. Variation of Specimen Temperature, to Nearest Whole Digit, with True Strain for Two Strain Rates, 0.125 s^{-1} and 100 s^{-1}; Temperature Measured *via* Thermocouple Welded to Gage Section of Tensile Test Specimen

	Temperature (°C)	
Strain	Strain Rate 0.125 s^{-1}	Strain Rate 100 s^{-1}
0	24	24
0.05	29	30
0.10	35	37
0.15	42	45
0.20	50	53
0.25	59	63
0.30	69	73
0.35	80	85

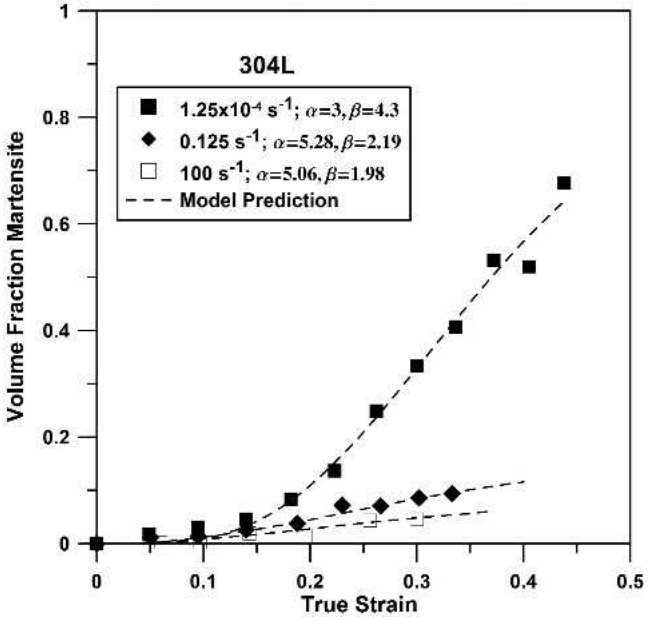

Fig. 18—Predicted variation of volume fraction α'-martensite with true strain for 304L, from Eq. [5], and corresponding experimental data. Values of α and β at 24 °C, at the start of deformation, are shown.

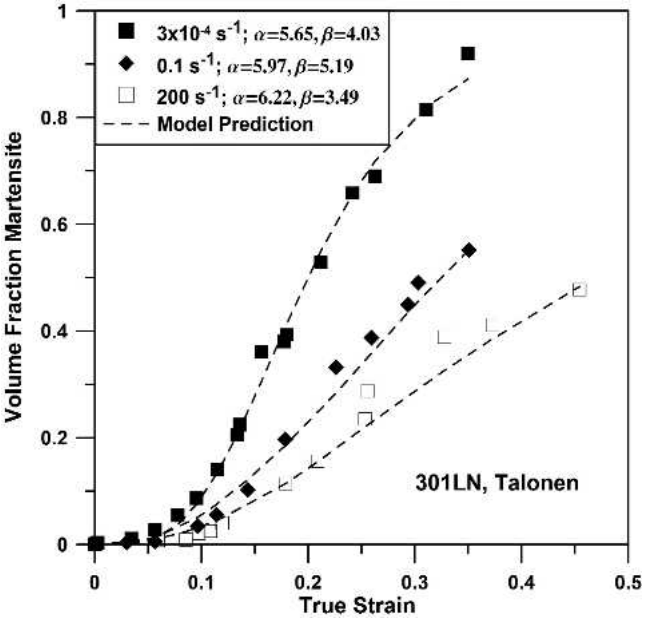

Fig. 19—Predicted variation of volume fraction α'-martensite with true strain for 301LN, from Eq. [5], and corresponding experimental data for 301LN.[20] Values of α and β at 24 °C, at the start of deformation, are shown.

IV. CONCLUSIONS

1. Both austenitic stainless steels, 309 and 304L, experience increasing yield strengths as the strain rate is increased from 1.25×10^{-4} s^{-1} to 400 s^{-1}. The yield strength of 309 increases from 291 to 541 MPa. The yield strength of 304L increases from 300 to 480 MPa.
2. The UTS of 309 increases from 639 to 791 MPa as strain rate is increased from 1.25×10^{-4} s^{-1} to 400 s^{-1} due to a positive strain rate sensitivity. On the contrary, the UTS of 304L is greatest at the lowest strain rate, 755 MPa, where isothermal conditions prevail and the strain-induced transformation of austenite to martensite operates uninhibited. As strain rate is increased to 0.125 s^{-1}, the UTS of 304L decreases from 755 MPa to a minimum value, 646 MPa, because the heat from deformation is retained in the tensile sample. The test is assumed to be adiabatic at this rate. Increased temperature inhibits the transformation because of the associated greater austenite stability as well as the reduction in nucleation sites due to more nonplanar slip. As strain rate is increased further, UTS increases as it does for 309, reaching 738 MPa at 400 s^{-1}.
3. The UEL values of both steels follow a similar trend with high elongations at the lowest strain rate, 47.9 pct for 309 and 59.1 pct for 304L, where isothermal conditions prevail. As the rate is increased to the point where deformation occurs adiabatically, 0.125 s^{-1} in this study, the values drop to a minimum, 31 pct for 309 and 42.1 pct for 304L. The decrease is attributed to localized heating in incipient necks in the tensile specimen and a resultant local thermal softening causing local instability. The loss of UEL over this range is more severe for 304L because, in addition to thermal softening, the strain-induced martensitic transformation, which acts to stem neck formation because of its relative strength, is inhibited by temperature increase. As strain rate is increased further, UEL increases moderately, to 35.2 pct for 309 and 45.9 pct for 304L, probably due to strain rate sensitivity.
4. The effect of increasing strain rate and associated heating of the specimen on mechanical behavior of 304L is distinctly demonstrated by the variation of work-hardening rate with strain. At a strain rate of 1.25×10^{-4} s^{-1}, the work-hardening rate increases dramatically, from approximately 1750 MPa/unit strain, starting at about 0.1 strain, and peaks at a value of 2250 MPa/unit strain at about 0.3 strain. At 0.45 strain, the value is again low, about 1200 MPa/unit strain. The strong secondary hardening effect at intermediate levels of strain results in high UTS and UEL compared to the stable 309 alloy, which exhibits no secondary hardening and relatively low values of work hardening. For example, at 0.3 strain, the work-hardening rate is approximately 1200 MPa/unit strain, independent of strain rate. As strain rate is increased and specimen heating occurs, the work-hardening rate in 304L is less dramatic and differences in UTS and UEL between the two alloys are reduced.
5. Progression of the transformation of austenite to martensite with increasing strain has been modeled for both isothermal and nonisothermal tensile deformation using the kinetic equation from Olson and Cohen[1] and the functionality of the equation coefficients with temperature from Kumar and Singhal.[37] The transformation behavior of 304L and 301LN from Talonen *et al.*[20] was also modeled and the equation coefficients were found to rank with austenite stability and SFE, as proposed by Olson and Cohen. Use of the modeling technique developed here in combination with finite-element predictions of temperature, strain, and strain rate gradients in, for example, structural automotive members undergoing crash scenarios should provide an ability to model the evolution of martensite, strength, and energy absorption during deformation of the previously mentioned alloys.

ACKNOWLEDGMENTS

The authors thank the Advanced Steel Processing and Products Research Center at the Colorado School of Mines for support of this work as well as AK Steel for supplying the steels. The guidance of Dr. Robert Comstock, AK Steel, as well as Professor David Matlock and Dr. Amar De, Colorado School of Mines, is very much appreciated. Also, the authors thank Ms. Pallas Papin and Ms. Ann Kelly, both of the MST-6 Group at Los Alamos National Laboratory, who provided expertise in microprobe analysis and metallography, respectively.

REFERENCES

1. G.B. Olson and M. Cohen: *Metall. Trans. A*, 1975, vol. 6A, pp. 791-795.
2. A.H. Eichelman and F.C. Hull: *Trans. ASM*, 1953, vol. 45, pp. 77-104.
3. T. Angel: *J. Iron Steel Inst.*, 1954, vol. 177, pp. 165-74.
4. K. Nohara, Y. Ono, and N. Ohasi: *J. Iron Steel Inst. Jpn.*, 1977, vol. 63, pp. 772-82.
5. J.A. Venables: *Phil. Mag.*, 1962, vol. 7, pp. 35-44.
6. R. Lagneborg: *Acta Metall.*, 1964, vol. 12, pp. 823-43.
7. P.L. Mangonon and G. Thomas: *Metall. Trans.*, 1970, vol. 1, pp. 1577-86.
8. R.P. Reed and C.J. Guntner: *Trans. TMS-AIME*, 1964, vol. 130, pp. 1713-20.

9. E. Nagy, V. Mertinger, F. Tranta, and J. Solyom: *Mater. Sci. Forum*, 2003, vols. 414–415, pp. 281-88.
10. A. De, D.C. Murdock, M.C. Mataya, J.G. Speer, and D.K. Matlock: *Scripta Mater*., 2004, vol. 50, pp. 1445-49.
11. J.W. Brooks, M.H. Loretto, and R.E. Smallman: *Acta Metall*., 1979, vol. 27, pp. 1829-38.
12. J.W. Brooks, M.H. Loretto, and R.E. Smallman: *Acta Metall*., 1979, vol. 27, pp. 1839-47.
13. W.-S. Lee and C.-F. Lin: *Metall. Mater. Trans. A*, 2002, vol. 33A, pp. 2801-10.
14. J.P. Bressanelli and A. Moskowitz: *Trans. ASM*, 1966, vol. 59, pp. 223-39.
15. G.L. Huang, D.K. Matlock, and G. Krauss: *Metall. Trans. A*, 1989, vol. 20A, pp. 1239-45.
16. S.F. Peterson, M.C. Mataya, and D.K. Matlock: *JOM*, 1997, vol. 49 (9), pp. 54-58.
17. C. Tague: Master's Thesis, Colorado School of Mines, Golden, CO, 1999.
18. S.S. Hecker, M.G. Stout, K.P. Staudhammer, and J.L. Smith: *Metall. Trans. A*, 1982, vol. 13A, pp. 619-26.
19. L.E. Murr, K.P. Staudhammer, and S.S. Hecker: *Metall. Trans. A*, 1982, vol. 13A, pp. 627-35.
20. J. Talonen, P. Nenonen, G. Pape, and H. Hanninen: *Metall, Trans. A*, 2005, vol. 36A, pp. 421-32.
21. R.E. Schramm and R.P. Reed: *Metall. Trans. A*, 1975, vol. 6A, pp. 1345-51.
22. "Standard Practice for X-ray Determination of Retained Austenite in Steel with Near Random Crystallographic Orientation," *ASTM Standard E975-03*, vol. 03.01, ASTM, Philadelphia, PA, 2003, p. 741.
23. B.D. Cullity and S.R Stock: *Elements of X-Ray Diffraction*, 3rd ed., Prentice Hall, Upper Saddle River, NJ, 2001, pp. 396-99.
24. R. Jackson: in *Sheet Metal Forming and Energy Conversion*, ASM, Metals Park, OH, 1977, pp. 264-84.
25. D.V. Neff, T.E. Mitchell, and A.R. Troiano: *Trans. ASM*, 1969, vol. 62, pp. 858-68.
26. M.G. Stout and P.S. Follansbee: *J. Eng. Mater. Technol.-Trans. ASME*, 1986, vol. 108, pp. 344-53.
27. W. Lee and C. Lin: *Mater. Sci. Eng*., 2001, vol. A308, pp. 124-35.
28. J.D. Campbell: *Mater. Sci. Eng*., 1973, vol. 12, pp. 3-21.
29. A.R. Dowling, J. Harding, and J.D. Campbell: *J. Inst. Met*., 1970, vol. 98, pp. 215-24.
30. P.S. Follansbee, G. Regazzoni, and U.F. Kocks: *Mechanical Properties at High Rates of Strain*, The Institute of Physics, Bristol, United Kingdom, 1984, pp. 71-80.
31. P.S. Follansbee: *Int. Conf. on Metallurgical Applications of Shock-Wave and High-Strain Rate Phenomena (EXPLOMET '85)*, Marcel Dekker, New York, NY, 1986, pp. 451-79.
32. J. Talonen, P. Nenonen, and H. Hanninen: *7th Int. Conf. on High Nitrogen Steels*, N. Akdut, B.C. De Cooman, and J. Foct, eds., GRIPS Media, Bad Harzberg, Germany, 2004.
33. R.W. Rathbun, D.K. Matlock, and J.G. Speer: *Scripta Mater*., 2000, vol. 42, pp. 887-91.
34. K.P. Staudhammer, L.E. Murr, and S.S. Hecker: *Acta Metall*., 1983, vol. 31, pp. 267-74.
35. P.J. Ferreira, J.B. Vander Sande, M. Amaral Fortes, and A. Kyrolainen: *Metall. Mater. Trans. A*, 2004, vol. 35A, pp. 3091-3101.
36. K. Sugimoto, M. Kobayashi, and S. Hashimoto: *Metall. Trans. A*, 1992, vol. 23A, pp. 3085-91.
37. A. Kumar and L.K. Singhal: *Metall. Trans. A*, 1989, vol. 20A, pp. 2857-59.